DIAGNOSTIC TEST-BEAM-LINE FOR THE MESA INJECTOR*

I. Alexander†, K. Aulenbacher, V. Bechthold, B. Ledroit, C. Matejcek
Institut für Kernphysik, Johannes Gutenberg-Universität, D-55099 Mainz, Germany

Abstract

With the test-beam-line it is possible to measure the two transverse phase-spaces and the temporal distribution of the electron bunches. It is also possible to investigate the emittance close to the source and further down stream to check the emittance evolution along the beam-line. Further more the beam halo can be studied. The beam-line components will be introduced and some preliminary results will be presented.

INTRODUCTION

MESA will be a multi-turn Energy Recovery Linac (ERL) which can be operated in two different modes. An ERL Mode (105 MeV) or an External Beam (EB) Mode (155 MeV) [1, 2]. The source will be a 100 keV dc photo gun which delivers polarized electrons with a current of 150 µA and an unpolarized electron beam with a beam current of 1 mA in stage 1 and 10 mA in stage 2. Close to the source there will be a spin manipulation section with two Wien-Filters and a solenoid followed by a chopper-buncher section consisting of four normal conducting cavities. The injector will be normal conducting with an output energy of 5 MeV. After the injector follow two superconducting linac modules which produce an energy gain of 25 MeV each. In Figure 1 a view of MESA is shown. The goal is to operate in cw-mode which means a bunch charge of 0.8 pC in stage 1 and 8 pC in stage 2.

The task of the diagnostic test-beam-line is to determine if the source can deliver a smaller emittance than the acceptance of the accelerator - for all bunch charges - which requires that the normalized emittance is $\varepsilon_n \leq 1\,\mu\text{m}$. For the operation of MESA the source should be reliable and deliver a high extractable charge with a long lifetime.

Semiconductor photo cathodes have some properties that should be taken into account. Close to the band gap energy it is possible to create spin polarized electrons with circular polarized photons. However when operating in this mode one suffers from low quantum efficiency (QE) and reduced cathode lifetime. If high currents, but no spin-polarization, are desired it is advantageous to use higher photon energies, since the QE is almost an order of magnitude larger and the lifetime is longer. At around 400 nm the photo cathodes can have a QE of $10\% \triangleq 32\,\text{mA/W}$. For higher photon energies not only the QE increases but also the thermal emittance does. This is because of the fact, that the stimulated electrons have not enough time to thermalize while they are traveling through the semiconductor and end up with a wider energy distribution. This additional energy spread gets transferred into more transverse momenta which leads to a higher thermal emittance [3].

The source in the diagnostic test-beam-line has delivered 700 C within one charge-lifetime at average currents exceeding 1 mA (MESA stage-1). The experiment needs average current of 1(10) mA corresponding to an extracted charge of 3.6(36) C/h if a transmission of 100% is assumed. To achieve a complete transmission a RF-synchronized laser must excite photo-emission. We will capture the so-produced bunches by a harmonic buncher system which can accept bunches with an extension of about 120°. This leads to the requirement that the emitted intensity - which is the convolution of the temporal laser intensity profile and the response of the photo cathode - must fit into this interval. Tiny fractions outside the interval may be suppressed by a chopper system to provide very clean operating conditions for MESA. In the set-up described here one of the circular deflecting cavities which were developed for the chopper system of MESA is used as temporal diagnostic instrument - see below.

We estimate the space charge caused current limit of the source by $I_{sc,lim} = p_0 \frac{A}{d^2} U^{3/2}$. Here $p_0 = 2.33 \cdot 10^{-6}\,\text{A/V}^{3/2}$ is the so-called perveance, $\frac{A}{d^2} = 44.4 \cdot 10^{-6}$ is a geometric factor with the emitting area $A = 1\,\text{mm}^2$ and the cathode-anode distance $d = 150\,\text{mm}$. The accelerating voltage $U = 100\,\text{kV}$. With all these parameters the emittance is still $< 1\,\mu\text{m}$ and the current limit would be $I_{sc,lim} \simeq 3\,\text{mA}$. This leads to the expectation, that the source can fulfill the requirements of MESA stage 1. This is also supported by CST-computersimulations [4]. Nevertheless a new 200 keV source is in production to increase the current limit to the requirements of MESA stage 2 [4].

COMPONENTS

Beam Line

A schematic overview of the beam-line setup is given in Figure 2. In the upper left side there is the dc photo gun with 100 kV and the electrons get accelerated in the vertical direction. After 1 m of beam-line the first analyzing stage (scanner 1) is placed followed by an α-magnet which bends the electrons 270° from the vertical to the horizontal direc-tion. Scanner 1 is positioned close to the source so that it is possible to measure the emittance without large influence of other beam manipulating elements. Between the both α-magnets the second analyzing stage (scanner 2) is mounted.

*Work supported by the German Science Foundation (DPG) under the Cluster of Exelence PRISMA
†alexand@kph.uni-mainz.de

ISBN 978-3-95450-183-0

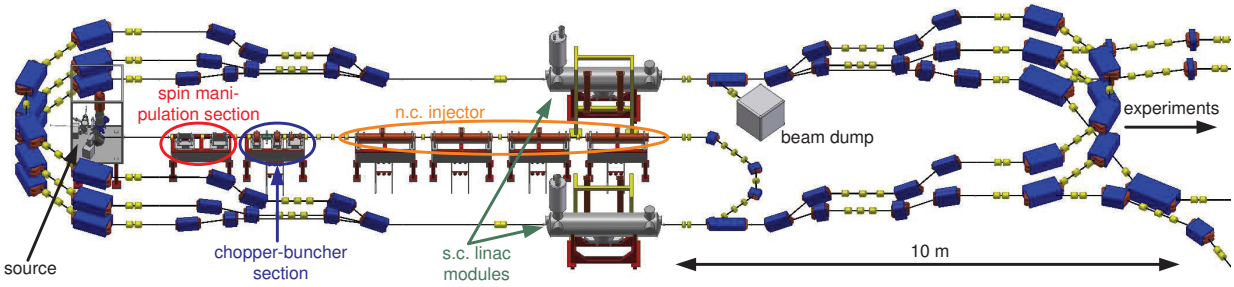

Figure 1: Floor plan of the MESA accelerator facility. In the left mid side sits the 100 keV dc photo gun, followed by some spin manipulation elements and the normal conducting injector. The main linac consists of two superconducting linac modules with two or three recirculations, depending on the operation mode. The experiments will be located further on the side and are not shown here to enhance visibility.

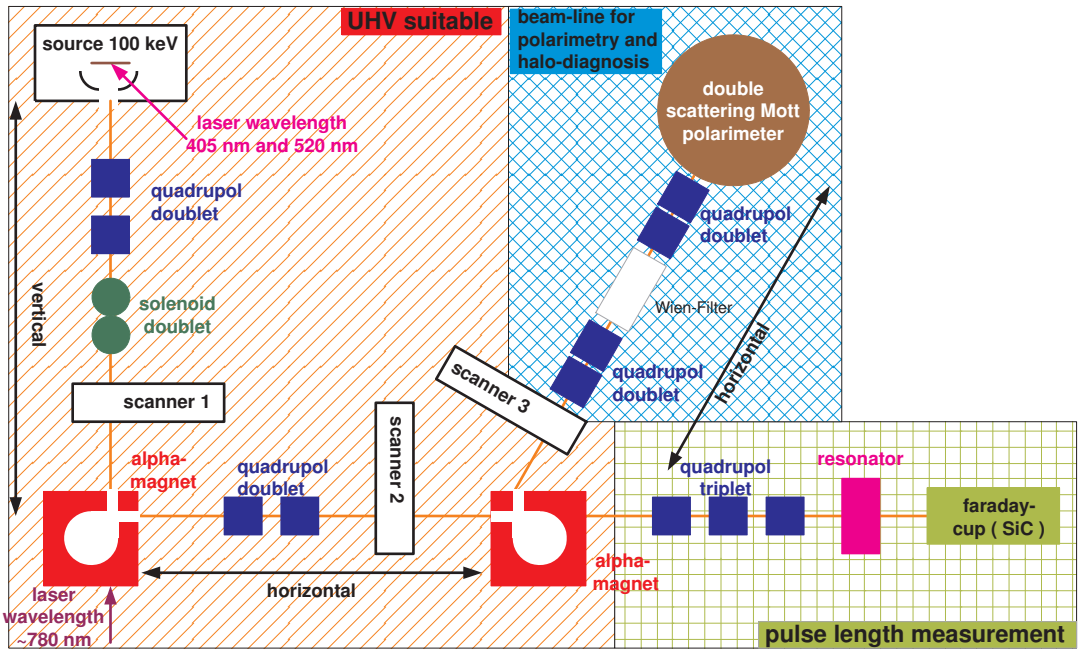

Figure 2: Schematic overview of the beam-line setup.

Here the evolution of the emittance with respect to the position of scanner 1 can be studied. If the second α-magnet is switched off investigations of the temporal distribution of the electron beam can be done with a deflecting cavity [5, 6, 7] and a Ce:YAG screen. If the second α-magnet is switched on the electrons pass by the third analyzing stage (scanner 3) where it is possible to take a closer look to the beam halo. Behind scanner 3 there is a Wien-Filter for spin manipulation and a double scattering Mott polarimeter. This device promises to yield very precise polarization measurements for the experiments foreseen at MESA. It is, however, not relevant for the contents discussed here, and we will therefore not discuss more details. All components between the source and the second α-magnet/scanner 3 are UHV compatible and bakeable. There are focusing elements like quadrupoles (blue) and solenoids (green) as well as several steering magnets which are not shown in Figure 2.

The UV-VIS laser system (405 & 520 nm) is installed on the "first floor" (2 m above ground) close to the source chamber to create a minimized beam spot on the photo cathode and due to the lack of space. For spin polarized electrons it is necessary to illuminate the photo cathode perpendicular to the surface with circular polarized laser light and because of that the IR laser system (780 nm) sits under the first α-magnet.

Laser System

The laser system consists of three laser diodes with dif-ferent wavelengths. The 405 nm and 520 nm laser diodes are mounted close to the source and illuminate the cathode through a view-port on the bottom of the source chamber. A schematic sketch is shown in Figure 3. At short distance after the two laser diodes there is an anamorphic prism pair

ISBN 978-3-95450-183-0

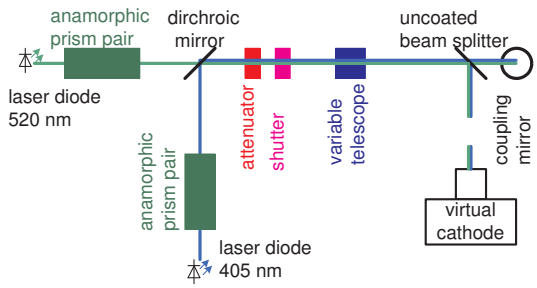

Figure 3: Overview of the UV-VIS laser system.

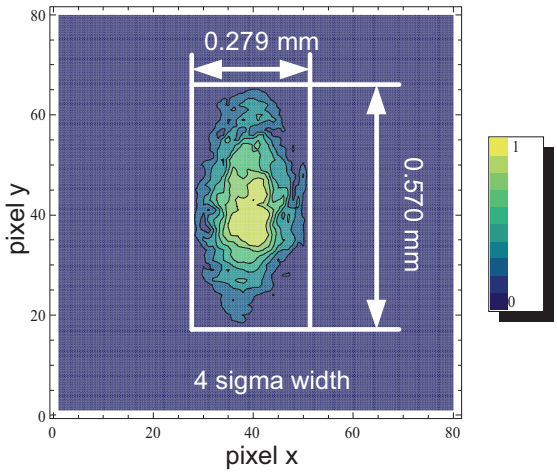

Figure 4: Example for the normalized intensity of a laser beamspot on the virtual cathode with a binning of 2 pixel in x and y.

to compensate the astigmatism of the diodes. After the prism pair a dichroic mirror to combine both wavelength is installed, followed by a remotely controlled attenuator and shutter. The next element is a variable telescope to create different beam spot sizes on the photo cathode. The penultimate element is an uncoated beam splitter which couples out 3% of the laser power and brings it onto a CCD-camera which works as virtual cathode to determine the beam spot size of the laser. The rest of the laser power gets reflected onto the photo cathode via a mirror. An example of the laser spot shape is given in Figure 4. This 2D plot shows the normalized intensity over the pixels of the camera which have a size of 6.6 µm. The IR laser system which is very similar to the UV-VIS system will be used to produce spin-polarized electron beam and is not shown here.

The laser system can be operated in three different modes. One is to create a dc beam. Here the maximum power and the average power are the same and below 300 mW. In the next mode it is possible to get dc pulse trains to decrease the thermal load on the screens. The pulses have a length of $10 - 200\,\mu s$ and a repetition rate of approximately 5 Hz. With this mode the average laser power can be decreased by a factor of 1000 but the maximum power remains the same. In the last operation

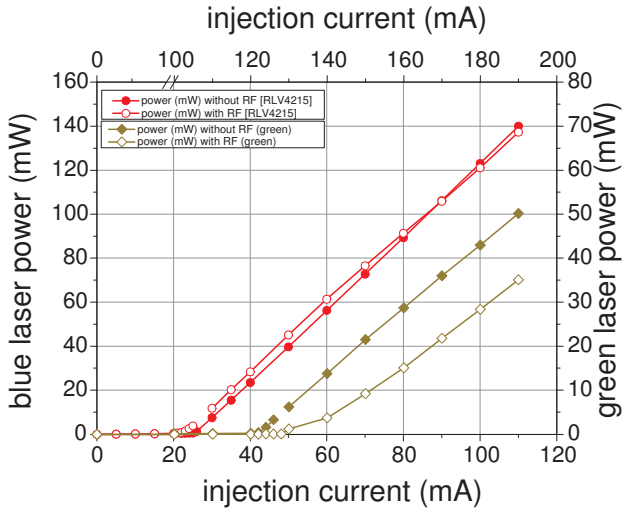

Figure 5: Average output power of a 405 nm laser diode and a 520 nm one plotted over the I_{inj}. Closed data points are for dc-current and opened ones are for dc-current and RF-power. The data for the blue laser diode belong to the left and the lower axis and for the green one to the right and the upper axis.

mode it can produce macro pulses by the superposition of the dc-current from the laser diode driver with additional RF-power up to 1.7 W. Measurements have shown that the average power remains the same as in mode 2 but the maximum power can be increased by a factor 5, depending on the pulsing behavior of the laser diode (see Figure 7). In Figure 5 is plotted the average output power of different laser diodes over the injection current (I_{inj}). The closed data points are for the dc-current and the open data points are with RF-power. The data for the blue laser diodes belong to the left and the lower axis and for the green one to the right and the upper axis. For the blue laser diodes it can be seen, that the RF-power shifts a little the threshold current and affects slightly the slope of the output power. But for the green laser diode the difference in the threshold current and the output power with and without RF is much higher. The slope of the output power for I_{inj} above 160 mA re-mains almost the same.

With this kind of measurement it can't be ensured that the laser diode is pulsing as wanted and thus, it is necessary to take a closer look to the pulse structure of the lasers. This can be done with a fast photo detector in the optical regime or with a deflecting cavity with the electron beam. The deflecting cavity transforms the longitudinal structure of the electron beam onto a transverse circle which can be observed over a screen behind the cavity. The bunch charges are too small to allow a single shot measurement, the picture represents many bunches which all impinge on the same area on the screen due to the synchronization between the cavity and the laser-system. A short description of the working principle of the deflector cavity is given in [5, 6, 7]. In Figure 6 we present two examples, one for

ISBN 978-3-95450-183-0

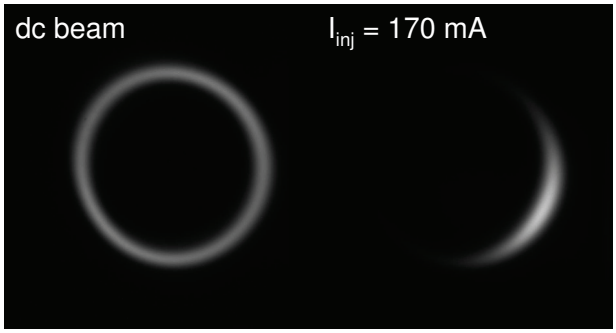

Figure 6: Example of pulse profiles behind the deflection cavity for dc beam (left) and RF-synchronized beam (right). The diameter is ˇ 30 mm with 120 W RF-power.

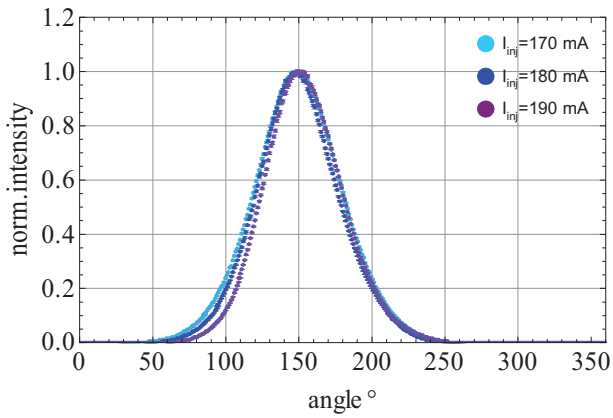

Figure 7: Normalized intensity profile for three different $Iinj$ of the green laser diode plotted over the RF-phase.

dc beam and the other one for RF-synchronized beam of the green laser diode. For this experiment a RF-power of 120 W was injected into the cavity to get a diameter of ≈ 30 mm. In Figure 7 the normalized intensity is plot-ted over the RF-phase of the cavity for three different I_{inj} (170, 180, 190 mA) of the laser diode. The peak power is more than five times larger than the the power measured at the same drive current in dc operation. All three I_{inj} deliver a transmission of 95% within a phase acceptance of 120°.

The green laser diode is mounted in the laser system to check how big the influence of the wavelength depending emittance is and if they show a better pulsing behavior than the blue ones.

Scanner Devices

All three scanners have a Ce:YAG screen with a diameter of 25 mm to optimize the beam trajectory and to make emittance measurements by quadrupole scans. Scanner 1 and 2 also contain tungsten wires with a diameter of 40 µm for emittance measurements and to investigate the halo distribution because of the higher dynamic range in comparison to the CCD-camera. Furthermore scanner 1 has two slit arrays which are oriented perpendicular to each other. They have a slit width of 25 µm and a spacing of 250 µm to make emittance measurements complementary to quad scan results. In scanner 2 the slits are replaced by a hole mask (pepper pot) with 21 x 21 holes with a diameter of 25 µm and a spacing of 250 µm in both directions. The purpose of scanner 3 is halo investigations and for that there are mounted two additional Ce:YAG screens. One with a 2 mm hole and the other one with a 3 mm hole.

RESULTS

Quad Scan

For the quadrupole scan the inverse focal length of one quadrupole is varied from $-5\,\mathrm{m}^{-1} \leq f^{-1} \leq 5\,\mathrm{m}^{-1}$ and the beam profile is obtained from a Ce:YAG screen with a CCD-camera. The squared beam diameter can be plotted over the k values of the quadrupole and on this data it is possible to fit a quadratic function which contains the TWISS parameters (α, β, γ). With this TWISS parameters the normalized emittance can be calculated as followed $\varepsilon_n = \beta_e\gamma_e\sqrt{\beta\gamma - \alpha^2}$ [8]. Here β_e & γ_e are the relativistic velocity and the Lorentz-factor of the electrons respectively.

This has been done for different beam alignment settings and the preliminary results are presented in Figure 8. In the upper right corner of the plot the dimensions of the used laser spot are shown and the beam profile is shown in Figure 4. With this dimensions of the emitting area $A = 0.5\,\mathrm{mm}^2$ the geometric ratio $\frac{A}{d^2} = 22.2 \cdot 10^{-6}$. The presented preliminary results are made with pulsed dc beam and without RF-synchronized pulses.

The results show large variations which may be caused by varying conditions, since they have been obtained over a long period of time. The increase in emittance can be expected because of the small perveance. However, further investigations are necessary before definitive statements can be made. In particular we will try to investigate the reason for differing values of the slit mask technique , presented below.

Slit Mask

In the slit mask emittance measurement method small slices of the beam are cut-out. More details of the slit mask method can be seen in [9]. This is presented on the left side of Figure 9 where the raw data of the measurement with 0.5 mA beam current are shown. Here the bit-value is plot-ted over the pixel position on the camera. From this data the width and the displacement of each peak are extracted and with this parameters it is possible to reconstruct the phase space distribution which can be seen on the right side of Figure 9. Here the color code and the point size indicates the normalized intensity of the slits. Furthermore with this parameters the normalized emittance can be calculated. In Figure 10 preliminary results for three different solenoid currents and a beam current of 0.1 mA to 0.5 mA are pre-sented. This data also represents the $1\sigma-$emittance. The variation of the solenoid current has been done to check

ISBN 978-3-95450-183-0

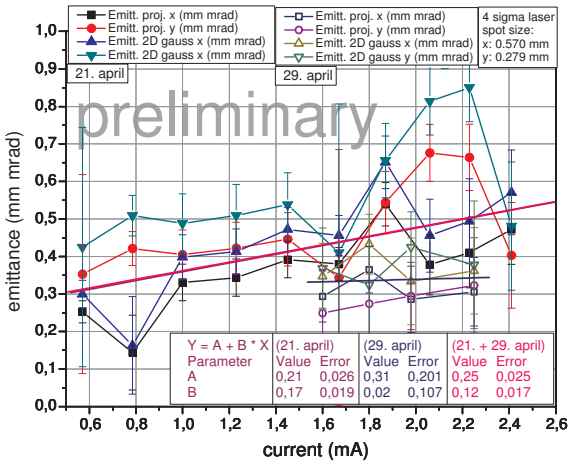

Figure 8: Preliminary emittance results from quadrupole scans are plotted over the beam current. The plot contains two different alignments and was made with pulsed dc beam. The results indicate fluctuations of the or-der of 30% the reasons of which are currently under investigation.

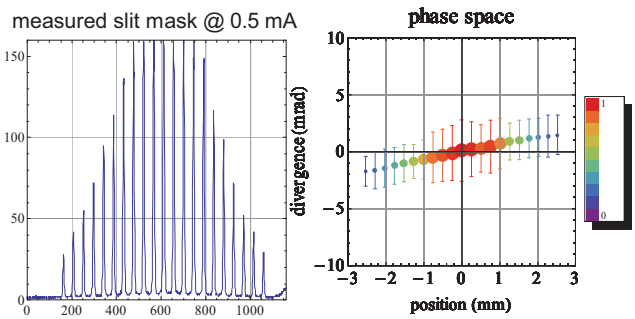

Figure 9: Raw data (left) and reconstructed phase space (right)measured with the slit mask. The color code and the point size indicates the normalized slit intensity.

if this has an influence on the emittance calculation. Up to now - unfortunately - it was not possible to measure with higher beam currents because of an accident where the photo cathode has lost a lot of QE. Nevertheless there is good reason to believe that in the near future slit mask measurements will be performed in the same current range as in Figure 8. This will clarify if the seeming increase in emittance is real and if it can be mitigated, for instance by increasing the perveance.

SUMMARY

The diagnostic test-beam-line is build up and ready to get used. Investigations of the two transverse phase-spaces with quadrupole scan technique and the determination of the beam profile with a screen or with wires are possible. The beam-line gives the possibility of a cross check be-tween quadrupole scan and slit mask measurements. The temporal distribution can be inspected with a deflecting

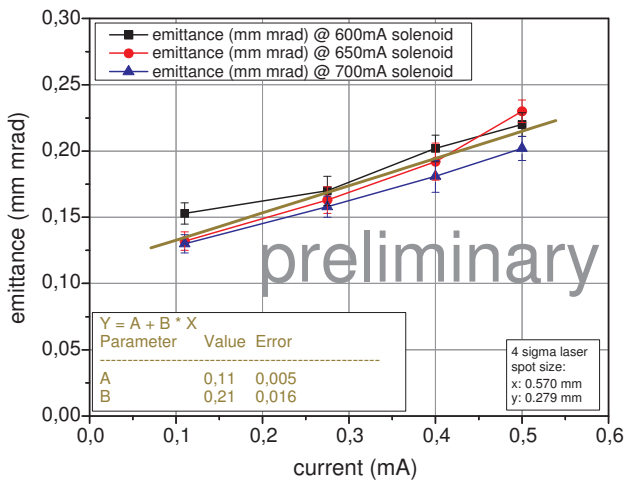

Figure 10: Preliminary emittance results from the slit mask mea-surements plotted over the beam current.

cavity that transforms the longitudinal distribution into an transverse one and deflects the beam onto a circle which can be observed with a Ce:YAG screen and a CCD-camera. All this can be done with three different laser wavelengths (405, 520, 780 nm) and for different laser spot sizes.

The first preliminary results of the emittance look promising to match the requirements of MESA stage 1. Further investigations of higher bunch charges etc. have to be done.

In the future it is planed to get more experience with the beam-line and the measurement techniques to characterize if the electron bunches from the source are suitable for MESA stage 1. Furthermore a closer look to helicity correlated halo effects is in preparation.

REFERENCES

[1] R. Heine, D. Simon, "Lattice and Start to End Sim-ulation of the Mainzer Energy Recovering Super-conducting Accelerator MESA", IPAC'14, Dres-den, Germany (2014), MOPRO108

[2] D. Simon, R. Heine, "Lattice and Beam Dynamics of the Energy Recovery Mode of the Mainzer Energy Recovering Superconducting Accelera-tor MESA", IPAC'15, Richmond, USA (2015), MOPWA046

[3] I. V. Bazarov, "Thermal Emittance And Response Time Measurement Of Negative Electron Affinity Photocathodes", Journal Of Applied Physics 103, 054901 (2008)

[4] S. Friederich, K. Aulenbacher, "Test electron source for increased brightness emission by near band gap photoemission", IPAC'15, Richmond, USA (2015), TUPWA044

[5] R. Heine, "Current Status Of The MESA Project", ERL2015, Stony Brook, USA (2015), WEIBLH1049

ISBN 978-3-95450-183-0

[6] V. Bechthold, "Eine Deflektor-Kavität für den MESA Beschleuniger", Diploma thesis, JGU Mainz, Germany (2013)

[7] B. Ledroit, "Hochfrequenzmessungen am Chopper-resonator für MESA", Bachelor thesis, JGU Mainz, Germany (2014)

[8] H. Wiedemann, "Particle Accelerator Physics", Springer, Germany (1993)

[9] M. Zhang, "Emittance Formula For Slits And Pepper pot Measurements", FERMILAB-TM 1988

ISBN 978-3-95450-183-0